This project has received funding from the European Union's Horizon 2020 research and innovation programme under grant agreement No 871813.

ICT Project No 871813

MUNDFAB

Modeling Unconventional Nanoscaled Device FABrication

D3.5: Final experimental results on epitaxy

P. Michałowski (Łukasiewicz-IMiF), R. Daubriac (CNRS), B. Sklenard (CEA), M. Opprecht (CEA), J.-M. Hartmann (CEA), P. Acosta Alba (CEA), S. Kerdilès (CEA), F. Cristiano (CNRS)

26.06.2023

Quality management

This deliverable was reviewed by:

A. La Magna (CNR-IMM)

C. Rossi (FhG-IISB)

Contents

Abstract

It has been demonstrated that with the increasing concentration of boron in SiGe layers the activation rate decreases. Thus, a series of post-epitaxy anneals experiments, particularly in sub-melt conditions, has been designed and carried out. However, it has been found that annealing in such conditions has a negligible effect on dopant activation.

1 Introduction

Due to the pandemic-related delays, **D3.3** “First batch of experimental results on epitaxy” was submitted in M20 and not M15 as previously expected. Thus, most of the experiments (i.e. Fabrication process, Optical analysis, Chemical analysis, Strain and defect characterizations and analysis, Boron activation analysis) have been already finished and reported in **D3.3**. Thus the only experimental activity remaining for the present deliverable is post-epitaxy anneals.

2 Post-epitaxy anneals

In standard processes, epitaxial growth is often followed by post-anneals, that can lead to negative effects as additional diffusion, dose loss, strain relaxation or to positive effects as defect annihilation. In this task, we performed post-epitaxy sub-melt laser anneals with different laser tools to assess the impact of such type of activation process on the electrical properties of *in situ* boron-doped strained-SiGe fabricated by CVD.

The layers were fabricated using a CENT300A epitaxy reactor from Applied Materials based on a recipe optimized in an Epsilon 3200A reactor from ASM. In order to create a p-n junction between the p-type Si substrate and the p-type SiGe layer, a lowly phosphorus-doped Si interlayer was deposited prior to the SiGe layer of interest. **Fig. 1 (a)** depicts the two similar systems fabricated by both epitaxy reactors, chronologically. For wafers dedicated to Task 3.4, on account of non-optimized and growth parameters variations between both epitaxy reactors, the substitutional concentration of phosphorus in the silicon interlayer was unintentionally increased from less than 10^{18} cm^{-3} to 10^{19} cm^{-3} (confirmed by SIMS measurements, **Fig. 1 (b)**).

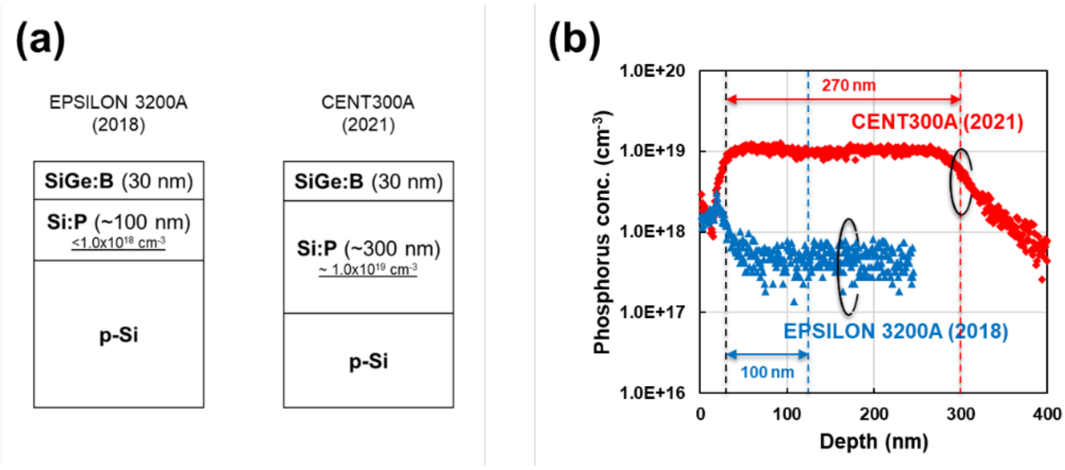

Fig. 1: (a) Schematic of both layer systems grown by epitaxy with two different reactors: Epsilon 3200A (2018) and CENT300A (2021). **(b)** SIMS measurements of phosphorus in both SiGe:B/Si:P/Si layers fabricated by both previously cited epitaxy reactors.

As a consequence, the space charge region extends towards the surface through the SiGe layer, making the electrical measurement of the interesting layer inconsistent. For this reason, layers fabricated inside CENT300A were not used for this study, and, to fulfil Task 3.4 within the agreed period, we decided to conduct our experiments on remaining layers previously fabricated inside Epsilon 3200A (as reported in **D3.3**). The *in situ* boron concentration of the SiGe layers we studied has been previously measured by SIMS to be ~2.3×10^{20} cm^{-3} and evaluated by Hall effect to be electrically active at ~60% (as reported in **D3.3**). This study aims to assess if subsequent sub-melt laser anneals may improve the initial activation level of the layer.

	Name	Type	Wavelenght (nm)	Pulse duration (ns)	Frequency (Hz)	Shot size (mm^2)
CEA-LETI	LT3100	Pulsed (XeCl)	308	160	4	15 x 15
CNR-UNIPD	COMPex 201F	Pulsed (KrF)	248	21	10	3 x 3
SCREEN LASSE	µs-LA	Pulsed	355	-	High frequency (cumulative)	10 x 10

Tab. 1: List of the laser tools used for T3.4.

Three different laser tools were used to perform the annealing process whose characteristics are listed in **Tab. 1**. Initially, as reported in D3.3, it was planned to perform continuous wave laser anneals (CNR-IMM) and furnace anneals (LAAS-CNRS). Both of them had to be canceled, the former as the laser tool broke down and the latter, for a question of time limit and priority. In this report, we will dedicate a sub-section for each laser tool to analyse separately all the found data and results.

2.1 SCREEN-LASSE (µs-LA)

The laser tool from LASSE-SCREEN is a microsecond UV-laser annealing platform based on the accumulation of short laser pulses at high frequency (considered as a quasi-continuous laser). The annealing temperature is controlled through two parameters, which are the energy density (ED) and the dwell time (DT). The DT is an indirect tuning parameter to minimize or maximize the cumulative feature of the laser. In other words, the longer the dwell, the more heat can be cumulated, the higher the maximum reached temperature will be. The first step of the design of experiment was dedicated to the melt threshold determination. To do so, six ED were selected (3.5 to 6.0 mJ/cm², with 0.5 mJ/cm² increment) and the DT was tuned until identifying the condition for which melted bands appear or disappear.

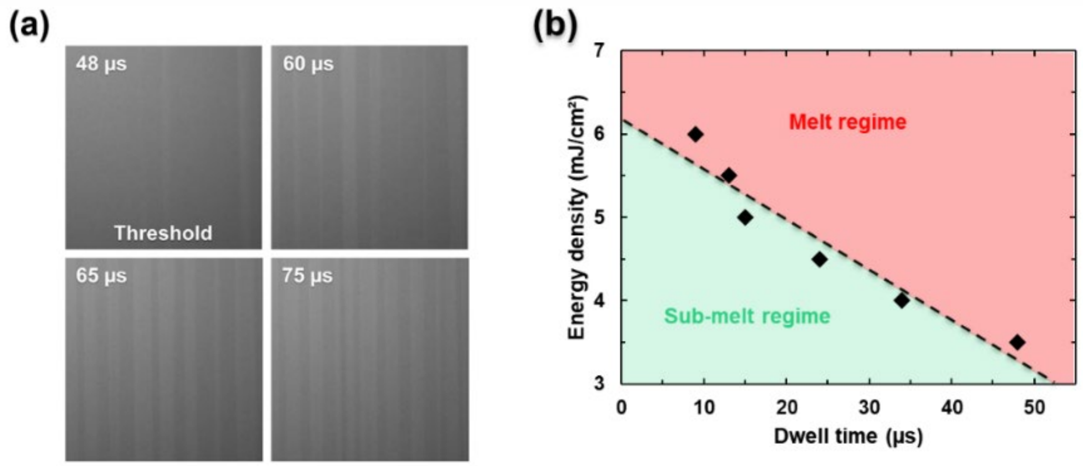

Fig. 2: (a) Camera images of annealed regions for melt threshold determination for a fixed ED of 3.5 mJ/cm² and various DT. The melt bands disappear below 48 µs DT. **(b)** Melt threshold as function of ED and DT.

The experimental procedure consisted of irradiating the samples with a given couple of laser annealing conditions (ED and DT) and then observing the sample with an embedded camera to determine the melting threshold (**Fig. 2 (a)**). Then the melting threshold is defined as the laser annealing conditions (couple of ED-IT values) which lead to the apparition of marks at the sample surface. For each ED, by increasing order, found DT corresponding to melt threshold conditions are respectively: 48, 34, 24, 15, 13 and 9 µs. These points have been plotted on **Fig. 2 (b)** and supposed to delimitate the sub-melt (green area) and melting regime (red area), illustrated by the dash line on **Fig. 2 (b).**

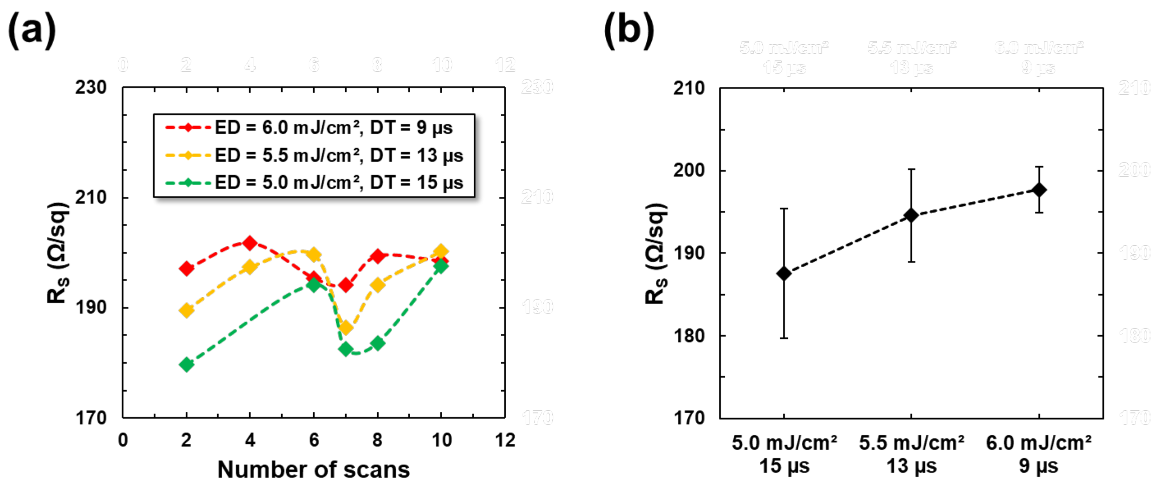

Fig. 3: (a) Sheet resistance as function of the number of scans for three different fixed laser conditions (ED and DT), confirmed to be in submelt laser regime by optical microscope observation. **(b)** Average sheet resistances with their respective standard deviation, calculated from multi-scans series.

Fig. 3 shows the sheet resistance (R_S) as function of different laser annealing conditions. Prior to the laser treatment, the post epitaxy R_S was measured around 190 Ohm/sq. It is observed that there is no significant drop of the sheet resistance (**Fig. 3 (b)**) for sub-melt conditions determined on **Fig. 2** (no apparition of marks at the sample surface). It is assumed that the marks appear at the sample surface before activating the sample in a solid-state regime (sub-melt). This can be attributed to a non-uniform distribution of the laser energy density within the irradiated area which leads to local melt and consequently mark apparition. Thus, the process window between full sub-melt activation and mark apparition (local melt) is narrow. However, optimization of laser annealing conditions should help to extend this process window and prevent the apparition of local melt.

2.2 CNR-UNIPD (KrF pulsed laser)

The laser tool used at University of Padua (Italy) is a COMPex 201F (Coherent) pulsed KrF laser operating at 248 nm with a pulse duration of 21 ns, and a frequency of 10 Hz (shot size: 3 x 3 mm²). When using multi-pulses conditions, the laser frequency is low enough to allow complete heat dissipation inside the material (non-cumulative). As for the previous laser, the first step has been dedicated to melt threshold identification. From previous studies **[1-3]**, it is known that roughness abruptly increases when reaching the surface melt regime. Therefore, AFM surface morphology measurements have been used to monitor the change of surface roughness corresponding to the melt regime. **Fig. 4** shows AFM images made on regions irradiated by one laser pulse at various ED, ranging from 0.410 to 0.827 J/cm².

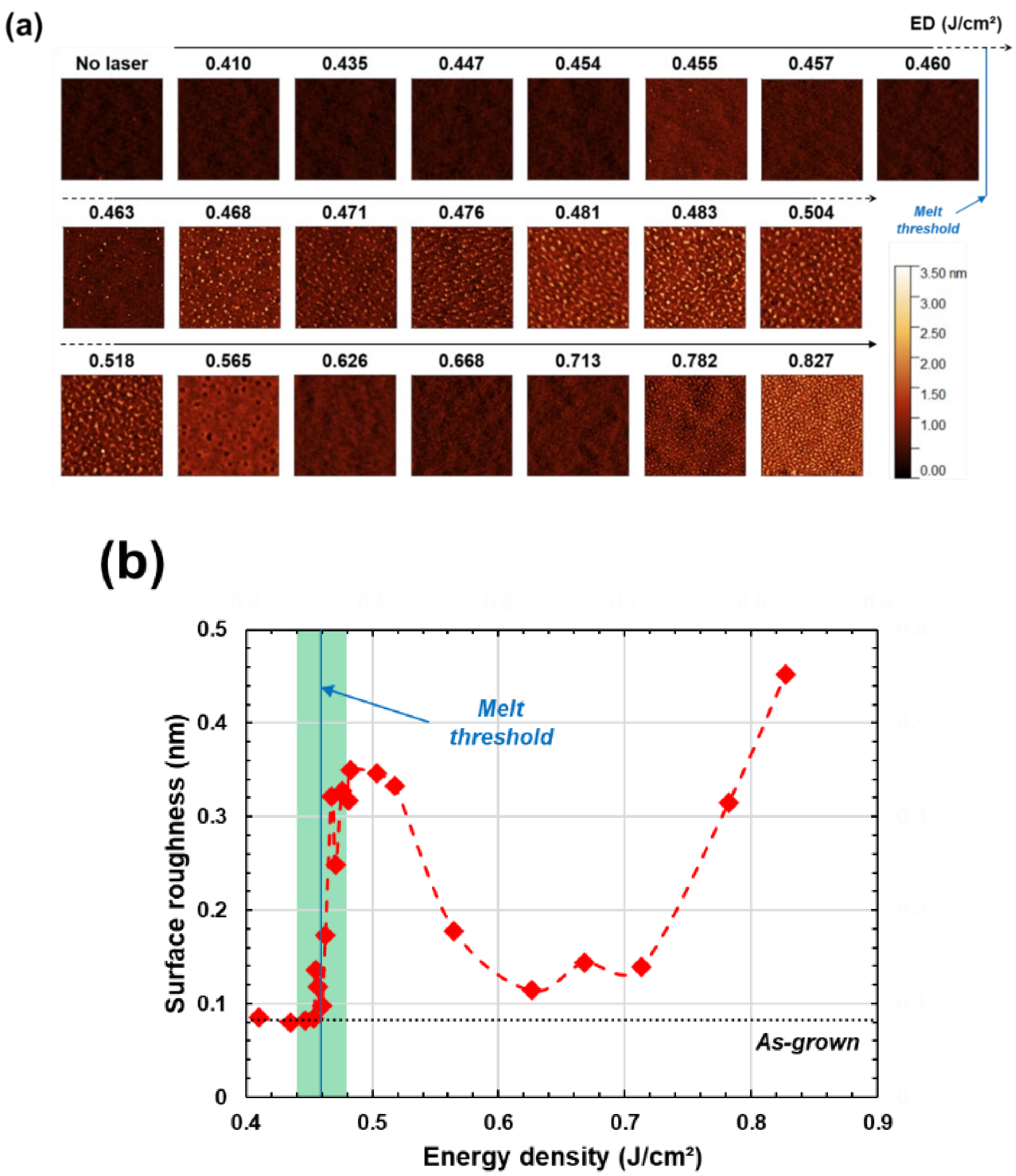

Fig. 4: (a) 1 x 1 µm² AFM images of surfaces irradiated with one laser pulse at ED between 0.410 and 0.827 J/cm² along with as-grown (no laser) condition. **(b)** Surface roughness as function of ED depicting the surface melt threshold. Green area indicates the ED range chosen for the submelt laser annealing design of experiment.

The melt threshold is evaluated between 0.460 – 0.463 J/cm². In order to anticipate melt threshold variations while still being near to it, we decided to cautiously explore ED between 0.440 and 0.480 J/cm² (0.01 J/cm² increment) with number of pulses of 1, 3, 30, 100 and 300 pulses. These conditions have been performed twice to ensure results reproducibility. Before preparing samples for electrical measurements, AFM images have been carried out to confirm the laser regime of our design of experiment's conditions. **Tab. 2** presents the corresponding regime for each laser condition region, determined by AFM. Sample 1 and 2 have 8 and 9 submelt regime conditions, respectively. For 1 laser pulse, results obtained from melt threshold determination series and both samples 1 and 2 series agree, giving a melt threshold ED between 0.46 – 0.47 J/cm². This melt boundary decreases when increasing the number of pulses, to reach a value between 0.44 – 0.45 J/cm² at 300 pulses.

Sample #1		Nb of pulses (-)				
		1	3	30	100	300
ED (J/cm^2)	0.44					AFM
	0.45	AFM	AFM	AFM	AFM	AFM
	0.46	AFM	AFM	AFM	AFM	AFM
	0.47	AFM				
	0.48	AFM				

Sample #2		Nb of pulses (-)				
		1	3	30	100	300
ED (J/cm^2)	0.44					AFM
	0.45	AFM	AFM	AFM	AFM	AFM
	0.46	AFM	AFM	AFM	AFM	AFM
	0.47	AFM				AFM
	0.48	AFM				

Submelt regime

Melt regime

Tab. 2: Laser regime as function of the ED and the number of pulses, determined by AFM measurements, for both highly doped SiGe:B samples annealed with KrF pulsed laser (CNR-UNPID).

Electrical measurements were performed using 1.6 mm-long cross-shaped Van der Pauw structures, fabricated thanks to a three steps process. The first two steps are using a photolithography process and are assigned to Van der Pauw structure shaping in combination with Reactive Ion Etching (RIE) and to aluminum contact deposition together with evaporation. The last procedure consists in applying a low-temperature furnace annealing process (H_2/N_2, 250°C, 2 h) to involve aluminum and silicon inter-diffusion and thus, to obtain symmetrical ohmic contacts **[4]**. Hall effects measurements achieved on both annealed samples are shown in **Fig. 5 (a-f)**. Results coming from submelt conditions have been highlighted using black contour. General trends for the three electrical parameters, namely the sheet resistance R_S, the Hall mobility μ_H and the Hall dose N_H are similar for both samples. The sheet resistance increases with the number of pulses while the Hall mobility remains unvaried and the Hall dose decreases. In the next paragraphs, two separated analyses will be provided for the submelt and surface melt regimes, respectively. Both of them will be based on the evolution of boron and phosphorus profiles, supported by schematics showed in **Fig. 6.** For surface melt regime conditions, although not being the main topic of T3.4, their associated results remain relevant as they are very close to submelt conditions.

For submelt conditions, the variations of electrical parameters with the number of pulses cannot be explained by the apparition of defects neither by an alloy stoichiometry modification, as reported in **D4.6**. Consequently, the unvarying Hall mobility is a clear evidence of an unchanged electrical concentration level, and so, that the slight increase of the sheet resistance and decrease of the Hall dose are induced by diffusion. Indeed, even when considering nanosecond scale anneals, temperatures approaching SiGe30% melt (~1215°C) are still very high and could be sufficient to involve interdiffusion of boron and phosphorus. The former is likely to diffuse of a few nanometres from the SiGe layer inside the n-type silicon buffer layer, and reversely for the latter. As a result, profiles will evolve from the left to the right schematic depicted in **Fig. 6**, thus leading to the extension of the space charge region inside the SiGe layer. In terms of physical parameters, the space charge region enlargement can be expressed by a reduction of the active dose (and so, of the Hall dose) and of the “electrical” thickness. Considering these variations in addition to a constant mobility and active concentration level, the sheet resistance $R_S = 1/q\mu Nt$ must increase, which is the case here (with q, the carrier charge).

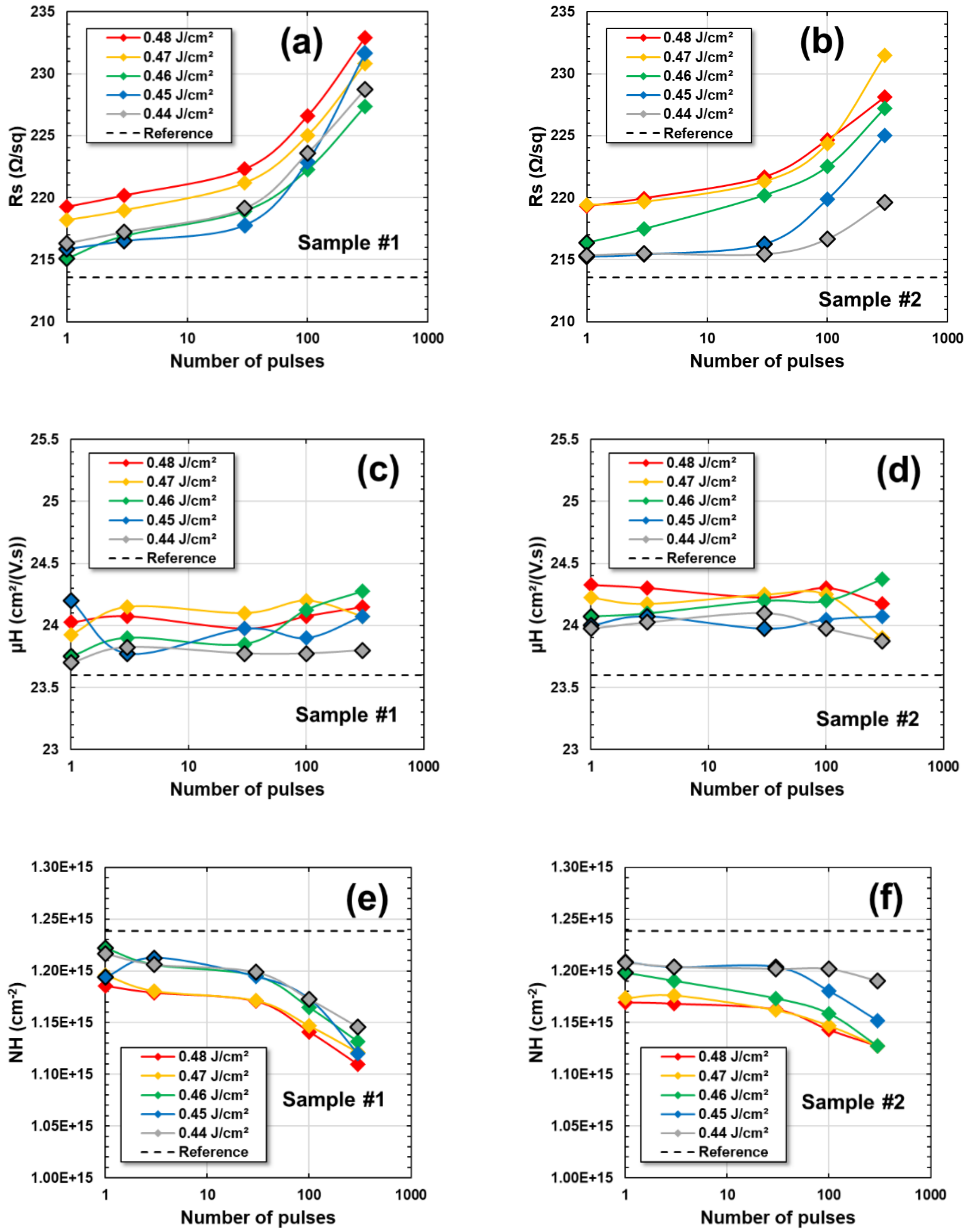

Fig. 5: Sheet resistance R_S **(a,b)**, Hall mobility μ_H **(c,d)** and Hall dose N_H **(e,f)** as function of the number of pulses at various ED, for both annealed SiGe:B samples, along with the electrical parameters of the reference layer (as-grown). Conditions corresponding to submelt regime (confirmed by AFM) have their symbol circled in black.

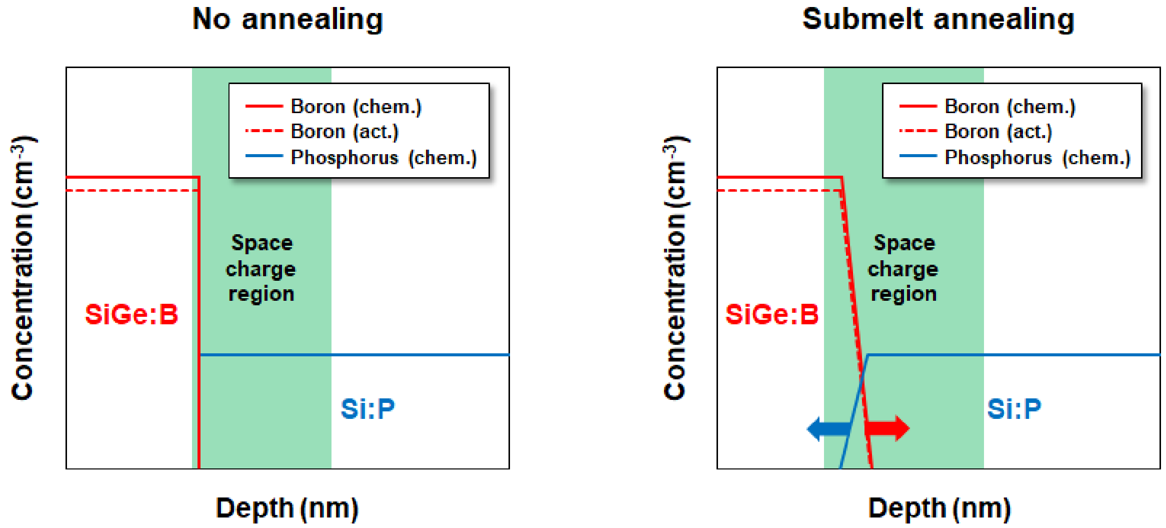

Fig. 6: Schematics of the expected evolution of the space charge region for all encountered conditions: as-grown (left) and submelt (right).

For surface melt conditions, the initial conditions to interpret the electrical results are different from submelt conditions. As presented in **Fig. 4 (a)**, this laser regime is a transition regime during which the laser conditions are not sufficient to form a continuous liquid layer. Instead, the melt of the SiGe layer happens locally and, is manifested by the apparition of droplet-shaped regions on the surface. As previously studied **[3]**, these melted regions can extend to 10 nm below the surface, involve local Ge redistribution and can generate partial relaxation inside the layer. From the same cited study and from AFM images analysis (**Fig. 7**), the ratio between the melted and non-melted area should be comprised between 0% and 20%, for the selected laser conditions. Consequently, in addition to previously mentioned phosphorus and boron interdiffusion, Ge redistribution and the supposedly induced SiGe partial relaxation must be considered in comparison to submelt conditions. Regarding the conversion of Hall electrical parameters into standard parameters, Ge local redistribution must be taken into account in the Hall scattering factor r_H. For Ge content ranging from 15% to 60%, the Hall scattering factor might vary between 0.35 to 0.50 for a strained SiGe layer and between 0.41 and 0.52 for a partially relaxed SiGe layer (see **D4.3**). Considering 10 nm-deep melted hillocks covering 20% of the surface, with only 5 nm involving significant change of the Ge content (ranging between 15 – 30%) **[3]**, and so, of the Hall scattering factor (~33% increase, from 0.35 to 0.47), the impact of such melted regions is equivalent to a 1 – 3% increase of r_H inside the SiGe layer, which does not impact the Hall dose and mobility trends. This means that the phosphorus-boron interdiffusion, that should be enhanced due to higher thermal budget than submelt conditions, overcompensates simultaneously the Ge local redistribution (so, the induced r_H variations) and the expected boron activation increase in the locally melted regions. For surface melt laser conditions, this results in shifted sheet resistances curves to higher values and Hall doses curves to lower values, in comparison to submelt laser conditions.

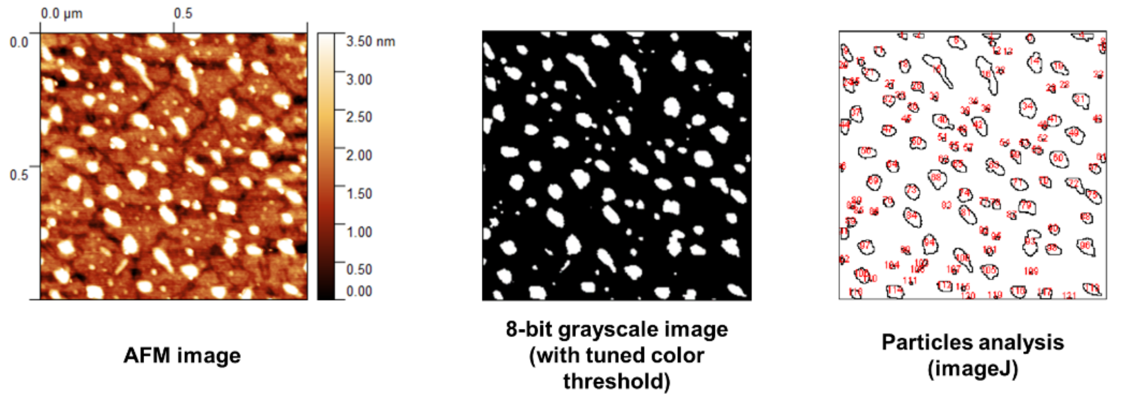

Fig. 7: Example of AFM image treatment with ImageJ software for the 0.46 J/cm²/300 pulses laser condition. From left to right: the raw AFM image of the surface morphology, then the 8-bit (grayscale) converted image and, the resulting display of particles analysis script, provided by ImageJ software.

2.3 CEA-LETI (LT3100)

The laser tool used at CEA-LETI (France) is a LT3100 (SCREEN-LASSE) pulsed XeCl laser functioning at a wavelength of 308 nm with a pulse duration of 160 ns and operating at a frequency of 4 Hz (shot size: 15 x 15 mm²). As well as for COMPex 201F from University of Padoue, given the low laser frequency, the multi-pulses laser mode is non-cumulative. The melt threshold was determined using time resolved reflectivity measurement combined with haze measurement. Based on this preliminary study, three ED were selected: 1.425 J/cm², 1.350 J/cm² and 1.200 J/cm², applied with number of pulses of 1, 3, 10, 30, 100, 300, 1000 and 3000. This design of experiment was repeated twice in order to have enough material for possible further analysis, for a total of 48 irradiated areas and 24 different laser conditions.

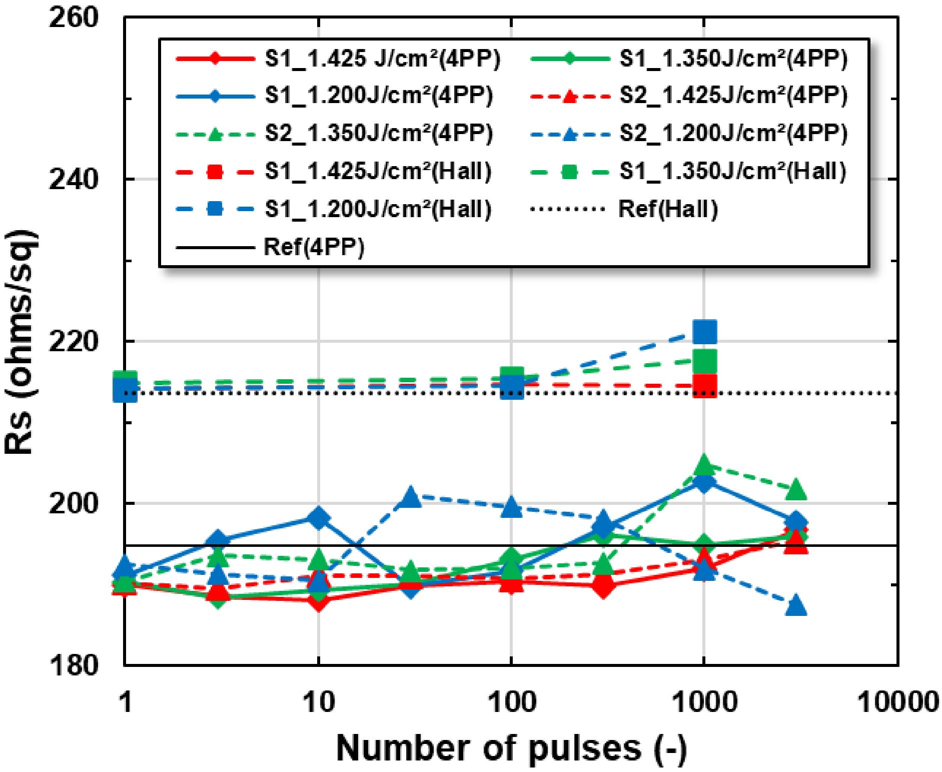

Fig. 8: Sheet resistance as function of the number of pulses for submelt annealed *in situ* boron-doped SiGe30% layer fabricated by CVD and measured by 4-point probe (4PP) method and Hall effect method

In **Fig. 8**, we compare the sheet resistance values obtained by using 4-point probe (4PP) and Hall effect (HE) measurements. We can first notice that the two sets of data extracted from both methods differs from each other. Without certainty, this might be explained by probe penetration during 4PP measurements and/or surface layer oxidation that occurred during the period in between the two measurement methods. Despite the observed sheet resistance shift, we can analyse both sets of data separately. For 4PP measurements, the sheet resistance values are fluctuating a lot around the reference value (194.8 ± 4.1 (2.1%) Ω/sq) for an average value of 193.1 ± 4.1 (2.1%) Ω/sq. This result suggests that the laser annealing process has no impact on the electrical properties of the initial layer, independently of the number of pulses. For Hall measurements, a slight divergence of the sheet resistance values can be noticed when reaching 1000 pulses. If this phenomenon was caused by diffusion (see data from COMPex 201F laser), the value deviation from reference value would have been expected to be more important for high thermal budget, i.e. high ED. In this case, the slight divergence in sheet resistance at 1000 pulses can be attributed to Hall measurement deviation. Indeed, the average extracted from Hall effect is 215.7 ± 4.1 (1.1%) Ω/sq which is comparable to reference value (213.6 ± 0.2 (0.1%) Ω/sq). Except the observed sheet resistance offset between 4PP and Hall measurement, the two sets of data show no impact of subsequent submelt laser annealing on electrical properties of *in situ* boron-doped SiGe30% layer. Hall mobility and dose have also been measured by Hall effect, in addition to sheet resistance (**Fig. 9**).

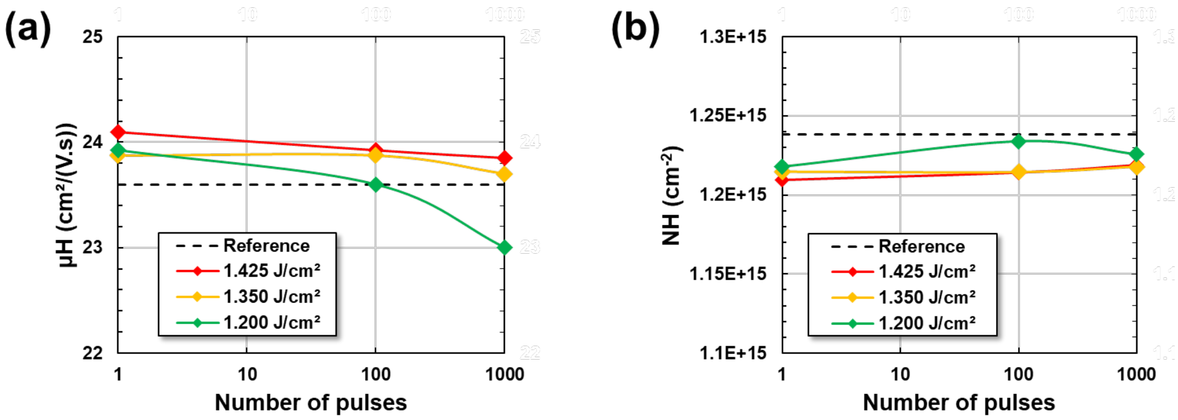

Fig. 9: Hall mobility **(a)** and Hall dose **(b)** as function of the number of pulses for submelt annealed *in situ* boron-doped SiGe30% layer fabricated by CVD and measured by Hall effect.

As well as for sheet resistance analysis, as variations are minor, we compare the average values of each Hall parameters with their respective reference value. The average Hall mobility and Hall dose have average values of 23.8 ± 0.3 (1.3%) $cm^2/(V.s)$ and $1.22 \times 10^{15} \pm 7.3 \times 10^{12}$ (0.6%) cm^{-2}, respectively, which are very similar to their reference value: 23.6 ± 0.1 (0.3%) $cm^2/(V.s)$ for the Hall mobility and $1.24 \times 10^{15} \pm 2.6 \times 10^{12}$ (0.2%) cm^{-2} for the Hall dose. Thus, Hall parameters do not show a clear impact of submelt laser annealing on electrical properties of *in situ* boron-doped SiGe30% layer.

Conclusions

In this report, we present results within the scope of Task 3.4 (WP3) that was devoted to post-epitaxy submelt anneals and their impact on the material properties, especially on dopant activation. To this end, laser annealing tools with different characteristics were used to evaluate the impact of pulse duration, wavelength, frequency and laser modes (single pulse, multi-pulses and multi-scans). Putting aside technical problems related to wafers fabrication and/or tool issues, the performed electrical measurements, whether by 4-point probe or Hall effect measurements, on submelt conditions (confirmed by available characterization methods) showed very low and even negligeable impact of such anneals on dopant activation of *in situ* boron-doped strained-SiGe30% grown by CVD.

Lab	Laser tool	Melt threshold determination	Design of experiment	Electrical measurements	Results/conclusions
SCREEN LASSE	µs-LA High frequency (cumulative)	Fixed ED Varying DT Characterization: Camera imaging Optical microscope	Single scan mode: 6 ED Varying DT Multi-passage mode: 6 ED/DT 2 – 10 scans	4PP	*Melt threshold shift due to non-uniform laser energy distribution within the irradiated area* For exploitable submelt conditions, electrical measurements show no impact of laser annealing on the electrical properties of SiGe:B layer
CNR UNIPD	COMPex 201F Pulsed KrF 248 nm 21 ns 10 Hz	Single pulse varying ED Characterization: AFM	5 ED 1 – 300 pulses	Hall effect	For both submelt and surface melt conditions, the slight evolution of electrical parameters can be explained by space charge extension inside SiGe:B layer, due to boron—phosphorus interdiffusion
CEA LETI	LT3100 Pulsed XeCl 308 nm 160 ns 4 Hz	Single pulse varying ED Characterization: TRR Haze	3 ED 1 – 3000 pulses	4PP Hall effect	For all studied conditions (submelt), Hall effect and 4PP measurements do not demonstrate a clear impact of the laser annealing on the electrical properties of SiGe:B layer *The shift in sheet resistance between 4PP and Hall effect methods remains unexplained*

References

[1] L. Dagault, P. Acosta-Alba, S. Kerdilès, J.-P. Barnes, J.-M. Hartmann, P. Gergaud, T. T. Nguyen, A. Grenier, J. Aubin and F. Cristiano, *Composition and Strain Evolution of Undoped $Si_{0.8}Ge_{0.2}$ Layers Submitted to UV-Nanosecond Laser Annealing*, ECS Transactions, Vol. 86, No. 7, pp. 29–39, 2018 (DOI: 10.1149/08607.0029ecst).

[2] L. Dagault, P. Acosta-Alba, S. Kerdilès, J. P. Barnes, J. M. Hartmann, P. Gergaud, T. T. Nguyen, A. Grenier, A. M. Papon, N. Bernier, *Impact of UV Nanosecond Laser Annealing on Composition and Strain of Undoped $Si_{0.8}Ge_{0.2}$ Epitaxial Layers*, ECS J. Solid State Sci. Technol., Vol. 8, No. 3, pp. 202–208, 2019 ([DOI: 10.1149/2.0191903jss).

[3] L. Dagault, *Investigation of Si1-XGex epilayers behavior upon ultraviolet nanosecond laser annealing*, PhD. thesis, p. 103, 2021.

[4] R. Daubriac, *Caractérisation de techniques d'implantations ioniques alternatives pour l'optimisation du module source-drain de la technologie FDSOI 28nm*, PhD. thesis, pp. 83 – 85, 2018.